N-cadherin and β1 integrin coordinately regulate growth plate cartilage architecture

Sydney E. Greer[a,b], Stephen J. Haller[a,b], Donghee Lee[b], and Andrew T. Dudley[a,b,*]
[a]Department of Genetics, Cell Biology, and Anatomy, and [b]Mary and Dick Holland Regenerative Medicine Program, University of Nebraska Medical Center, Omaha, NE 68198

ABSTRACT **Spatial and temporal regulation of chondrocyte maturation in the growth plate drives growth of many bones. One essential event to generate the ordered cell array characterizing growth plate cartilage is the formation of chondrocyte columns in the proliferative zone via 90-degree rotation of daughter cells to align with the long axis of the bone. Previous studies have suggested crucial roles for cadherins and integrin β1 in column formation. The purpose of this study was to determine the relative contributions of cadherin- and integrin-mediated cell adhesion in column formation. Here we present new mechanistic insights generated by application of live time-lapse confocal microscopy of cranial base explant cultures, robust genetic mouse models, and new quantitative methods to analyze cell behavior. We show that conditional deletion of either the cell–cell adhesion molecule *Cdh2* or the cell–matrix adhesion molecule *Itgb1* disrupts column formation. Compound mutants were used to determine a potential reciprocal regulatory interaction between the two adhesion surfaces and identified that defective chondrocyte rotation in a N-cadherin mutant was restored by a heterozygous loss of integrin β1. Our results support a model for which integrin β1, and not N-cadherin, drives chondrocyte rotation and for which N-cadherin is a potential negative regulator of integrin β1 function.**

Monitoring Editor
Rachel Brewster
University of Maryland, Baltimore County

Received: May 1, 2023
Revised: Dec 7, 2023
Accepted: Jan 23, 2024

SIGNIFICANCE STATEMENT

- During growth of long bones, daughter chondrocytes divide and rotate to form columns of proliferative chondrocytes. Previous studies showed a primary role for N-cadherin adhesion in cell rotation.
- Using mouse genetic models in conjunction with live tissue imaging, these studies show the surprising results of a key role for integrin adhesion in cell rotation and that heterozygosity for "Integrin beta-1" rescues architectural defects in N-cadherin–mutant growth plates.
- These results show a need for balance between cell–matrix and cell–cell adhesion to tissue architecture and provide crucial insights into mechanisms of growth disorders that could advance engineering of growth plate cartilage.

This article was published online ahead of print in MBoC in Press (http://www.molbiolcell.org/cgi/doi/10.1091/mbc.E23-03-0101) on January 31, 2024.

Conflicts of interest: The authors declare no financial conflict of interest.

Author contributions: S.G. and A.D. conceived and designed the experiments; S.G. and D.L. performed the experiments; S.G. and S.H. analyzed the data; S.G. and A.D. drafted the article; S.G. prepared the digital images; S.H. wrote software to analyze the imaging data.

*Address correspondence to: Andrew T. Dudley (andrew.dudley@unmc.edu)

Abbreviations used: AR, aspect ratio; Cdh2, cadherin-2/N-cadherin; Col2a1, collagen II alpha 1 chain; ECM, extracellular matrix; EGTA, ethylene glycol-bis(beta-aminoethyl ether)-N,N,N′; ENS, enteric nerv=ous system; Fgf, fibroblast growth factor; GFP, green fluorescent protein; HBSS, Hank's balanced salt solution; Hr, hours; HZ, hypertrophic zone; Ihh, indian hedgehog; ISS, intersphenoidal synchondrosis; Itgb1, integrin beta-1; LA/SA, ratio of long axis to short axis; MEM, modified Eagle's medium; mTmG, fluorescent cell membrane labeling reporter allele; PBS, phosphate buffered saline; PCR, polymerase chain reaction; PHZ, prehypertrophic zone; Pthrp, parathyroid hormone related peptide; PZ, proliferative zone; qPCR, quantitative polymerase chain reaction; RNA, ribonucleic acid; RT-qPCR, reverse transcription quantitative polymerase chain reaction; RZ, resting zone; SD, standard deviation; TBS, Tris buffered salineTBST, Tris buffered saline containing Triton X-100; Tgfb, transforming growth factor beta; Wnt, wingless/int-1.

INTRODUCTION

Bone growth is the product of cartilage growth and remodeling by endochondral ossification. For long bones and the cranial base, these processes are coordinately regulated in the growth plate cartilage, a specialized tissue that is organized into histologically and functionally distinct zones reflecting the distinct stages of chondrocyte maturation. The resting zone (RZ) is situated furthest from the site of ossification and is composed of many rounded, randomly arranged chondrocytes. Resting chondrocytes act as a reserve of stem-like precursors for chondrocytes in the adjacent proliferative zone (PZ), a region in which disk-shaped chondrocytes undergo clonal expansion to generate the characteristic columnar structure aligned with the growth vector (Dodds, 1930; Abad *et al.*, 2002; Mizuhashi *et al.*, 2018). After proliferating and extending the column, chondrocytes exit the cell cycle in the prehypertrophic zone (PHZ), enlarge in the hypertrophic zone (HZ), transdifferentiate into osteoblasts (Ono *et al.*, 2014; Yang, Zhu, *et al.*, 2014; Yang, Tsang, *et al.*, 2014; Zhou *et al.*, 2014) or undergo apoptosis, and prepare the cartilage matrix for mineralization (Hunziker & Schenk, 1989; Hunziker, 1994; Rosello-Diez & Joyner, 2015; Tsang *et al.*, 2015; Agirdil, 2020).

A key outstanding question is how growth potential is encoded in growth plates. Much of our current understanding of the process derives from studies of long bone development. Although bone growth is responsive to endocrine signals (Kronenberg, 2003; Rosello-Diez & Joyner, 2015; Lui *et al.*, 2018), growth plate transplantation experiments in rabbit showed that the age of the donor, not the host, determines growth rate (Stevens *et al.*, 1999). Likewise, transplanted salamander limb buds grow to the size defined by the donor and not the recipient (Harrison, 1924; Twitty & Schwind, 1931). Together, these observations suggest that the primary determinants of growth potential are intrinsic to the cartilage template. Studies from many laboratories have defined a central signaling feedback loop between parathyroid hormone related peptide (Pthrp) produced by resting chondrocytes and Indian hedgehog (Ihh) produced by prehypertrophic chondrocytes, as well as important contributions of the wingless/int-1 (Wnt), fibroblast growth factor (Fgf), and transforming growth factor beta (Tgfb) growth factor superfamilies. Although all long bones form from mesenchymal condensations of similar size (Hall & Miyake, 1992, 2000) and nearly identical hormones and growth factors regulate the developmental program (Kronenberg, 2003; Rosello-Diez & Joyner, 2015; Lui *et al.*, 2018), different long bones develop to distinct size and yet paired bones in bilaterally symmetric skeletons normally grow to nearly identical size.

Total growth is the integral of growth rate with respect to time, where column length (cell proliferation rate) and height of terminal hypertrophic chondrocytes are the primary correlates to growth rate (Sissons, 1955; Kember & Walker, 1971). We have been interested in elucidating how transit amplification of proliferative chondrocytes is regulated in the context of tissue architecture as disorganization of columns is often observed in disorders of longitudinal bone growth (Maeda *et al.*, 2007; Hirai *et al.*, 2011; Gibson & Briggs, 2016) with some notable exceptions (Ahrens *et al.*, 2011). We previously developed a live-cell imaging platform using cartilage explants from the cranial base, a growth plate of neuroectodermal origin that has some advantages for optical imaging over long bone growth plates. Using this system, we demonstrated a role for cadherin-mediated cell–cell adhesion by showing that treatment of cartilage explants with cadmium or EGTA, two validated inhibitors of cadherin adhesion, disrupted chondrocyte rotation in the proliferative zone (Romereim *et al.*, 2014). These findings were supported by similar results in the chick embryo using blocking antibodies to N-cadherin (encoded by *Cdh2*) and viral expression of a dominant-negative cadherin (Li *et al.*, 2017). Despite the strength of these complementary findings, it was previously known that cartilage-specific inducible genetic deletion of β1 integrin (encoded by *Itgb1*), a key subunit of ECM receptors on chondrocytes, resulted in similar phenotypes including disorganized proliferative columns (Aszodi *et al.*, 2003). However, the underlying mechanism generating the disorganized tissue architecture of *Itgb1* mutants was not determined as only standard histological sections were scored. Regardless, the similar observations in the cell adhesion pathway mutants highlights questions about the roles of cell–cell and cell–matrix adhesion surfaces in proliferative chondrocyte column formation.

The current study sought to determine the relative contributions of cadherin- and integrin-mediated cell adhesion in chondrocyte column formation by utilizing robust and specific genetic mouse models and advancements in image analysis capabilities that expand the available measures to quantify dynamic rearrangement behaviors and cellular phenotypes in mutant growth plate cartilage. Using these methods, we demonstrate that genetic deletion of *Cdh2* alters chondrocyte rotation and column formation as previously shown for nongenetic inhibition of cadherin function and that loss of *Itgb1* function produces a similar but more severe effect on chondrocyte rotation and column formation. We proposed the hypothesis that reciprocal regulatory interactions between the two adhesion surfaces coordinate chondrocyte rotation and column formation. To test this hypothesis, we analyzed an allelic series of *Cdh2* and *Itgb1* conditional mutants. Here, we present new evidence that suggests β1 integrin, not N-cadherin, is the driver of chondrocyte rearrangement and that N-cadherin potentially acts as a negative regulator of β1 integrin function. We propose the model that column formation requires fine-tuning of both N-cadherin–mediated cell–cell and β1 integrin–mediated cell–matrix adhesion and discuss how these processes might be regulated at the transition to initiate proliferative chondrocyte column formation.

RESULTS

Quantitative analysis of dynamic cell behaviors in wild-type growth plates

To measure dynamic events of column formation, we used a previously developed system for time-lapse confocal microscopy of cranial base explant cultures (Romereim *et al.*, 2014). The cranial base, or interspenoidal synchondrosis, is a flat growth plate tissue, which increases the number of chondrocytes within a field of view. Although distinct in origin from long bone growth plates (neural crest vs. mesodermal) and bidirectional in structure (Figure 1A) (McBratney-Owen *et al.*, 2008; Wei *et al.*, 2016), the cranial base growth plate displays similar tissue architecture, gene expression domains, and responses to growth factors consistent with growth plate cartilage in long bones, suggesting existence of evolutionarily conserved fundamental mechanisms underlying the unique structure of the growth plate (Chen *et al.*, 1999; Shum *et al.*, 2003; Young *et al.*, 2006; Koyama *et al.*, 2007; Nagayama *et al.*, 2008; Hsieh *et al.*, 2021; Unger *et al.*, 2021; Rignol *et al.*, 2022).

During mitosis, the centromeres and mitotic spindle of the discoid-shaped proliferative chondrocyte occupy a plane perpendicular to the division plane, the cellular interface formed during cytokinesis (Dodds, 1930). The primary measure of daughter cell rearrangement we use is rotation of the division plane, which is defined as the angle formed by the green fluorescent protein–labeled membrane at the interface of the two cells and a line drawn parallel

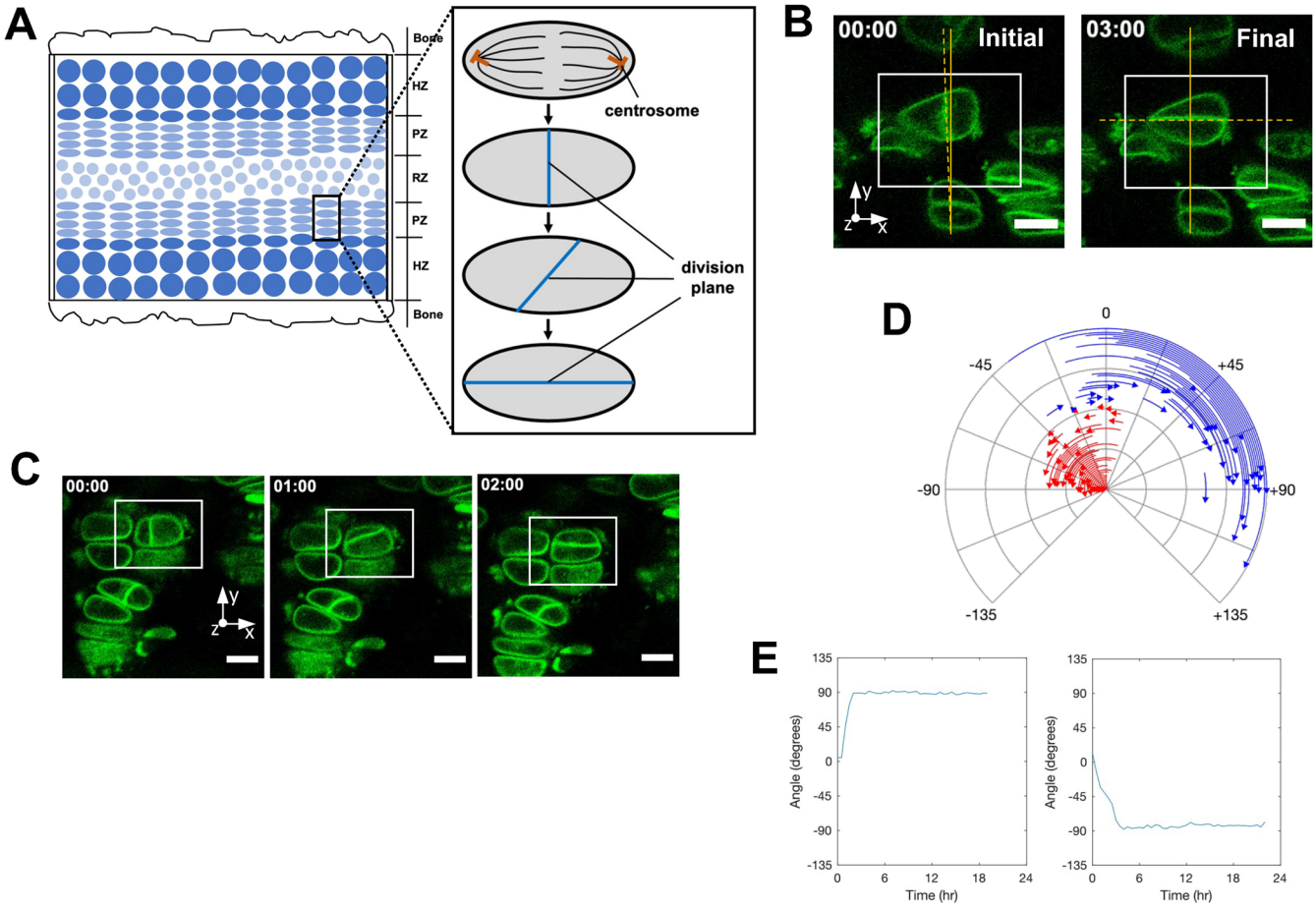

FIGURE 1: Experimental design and image analysis for time-lapse confocal imaging of wild-type cranial base growth plate. (A) Schematic diagram of murine intersphenoidal cranial base growth plate cartilage. The tissue is a bidirectional growth plate and is comprised of three major cartilaginous zones flanked with bone: resting (RZ), proliferative (PZ), and hypertrophic (HZ). Inset displays a proliferative chondrocyte with centrosomes at each pole forms a division plane (blue) following mitosis to create two daughter cells, which undergo a subsequent rotation. (B) The angles of division and final orientation of the division plane between daughter cells (dashed line) were quantified by defining the *y*-axis (solid line) as growth direction of the tissue and therefore parallel to nearby, already formed columns. (C) Time-lapse movie of proliferative zone dividing chondrocytes captures ~90-degree rotation behavior. (D) Angular trajectories for each wild type dividing cell starting with the initial division plane angle and projecting toward final rotation angle (arrowhead). (E) Examples of angular trajectories over time for single-cell rotations with a plateau around 90 degrees. $N = 82$ cells from 10 mice. Scale bar represents 10 μm.

to the long axis of the developing bone (Figure 1, A and B). As previous analysis was limited to measurement of the initial and final positions of the cell division plane, we developed a custom MATLAB code based on spline representations of daughter cells at every imaging time point to quantify additional variables and determine kinetic parameters (Supplemental Figure S1). For initial analyses, two independent observers performed measurements on a subset of images to demonstrate that user input did not affect results. Consistent with our previous findings, wild-type proliferative chondrocytes form an initial division plane parallel to the growth direction of the bone (*y*-axis of image) and undergo an ~90-degree rotation event to form a cell stack where the final division plane is perpendicular to the primary growth direction of the bone (Figure 1, C and D; Supplemental Video S1; Supplemental Figure S2). There is a strong bias in the initial division plane angle toward 0 degrees, and the final division plane angle has a bimodal distribution toward +90° or –90° (Figure 1D). Representative plots of single-cell trajectories undergoing rotation show an abrupt transition at cessation of rotation and stability of the division plane position after rotation has ended (Figure 1E).

Genetic models recapitulate known phenotypes

Previous studies demonstrated expression of cadherins and β1 integrin in the proliferative zone of growth plate cartilage using IHC and immunofluorescence (Aszodi *et al.*, 2003; Romereim *et al.*, 2014; Li *et al.*, 2017). Moreover, RNA-sequencing studies of growth plate chondrocytes fractionated into low cycling (resting) and high cycling (proliferative) populations demonstrate expression of *Cdh2* and *Itgb1* in both zones (Hallett *et al.*, 2021). We confirmed these findings in cranial base growth plate by demonstrating expression of N-cadherin and β1 integrin protein expression in both the resting and proliferative zones using immunofluorescence (Supplemental Figure S3). Thus, cranial base and long bone growth plate cartilage display comparable expression profiles of these cell adhesion molecules despite differences in developmental origin of the cartilage templates.

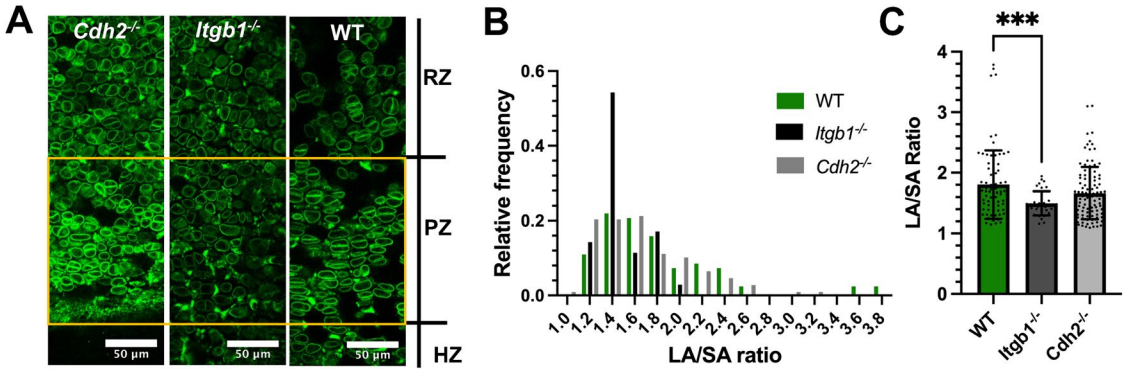

FIGURE 2: Loss of N-cadherin and β1 integrin create zonal disorganization defect. (A) Failure to form aligned clonal columns in proliferative zone of cranial base growth plates of *Cdh2*- and *Itgb1*-mutant mice. *Itgb1*-mutant cells appear more rounded in the proliferative zone as compared with WT and *Cdh2*. (B) Frequency distribution of the long axis to short axis ratio (LA/SA) of cells at the initial division time point with a bin size of 0.2. Rounded chondrocytes have a LA/SA ratio around 1, while discoid/flattened chondrocytes have a LA/SA ratio greater than 1. (C) *Itgb1*-mutant cells are more rounded than WT and *Cdh2* mutant cells, as defined by a shorter long axis to short axis aspect ratio. N (*Cdh2*) = 108 cells from 7 mice. *N* (*Itgb1*) = 35 cells from 4 mice. *N* (WT) = 82 cells from 10 mice. Comparisons of distributions of each mutant to the wild-type group in panel (C) performed using a two-tailed Kolmogorov–Smirnov Test. ***$p < 0.001$. Scale bar represents 50 µm.

Previously, we described a primary role for N-cadherin adhesion in chondrocyte rearrangement and column formation based on experiments using less specific inhibitors of total cadherin adhesion (Romereim *et al.*, 2014). Therefore, we turned to mouse genetic models to disrupt N-cadherin–dependent adhesion using a tamoxifen-inducible deletion of N-cadherin (*Cdh2*) and a Col2a1-creER^T transgene in conjunction with an mTmG reporter allele (Supplemental Table 1) (Feil *et al.*, 1997; Kostetskii *et al.*, 2005; Nakamura *et al.*, 2006; Muzumdar *et al.*, 2007). In addition, we generated an analogous mouse line for a conditional allele of the beta-1 subunit of integrin receptors (*Itgb1*). Confocal microscopy of cranial base explants from embryonic day (E) 17.5 mice following induction of recombination by daily tamoxifen injection from E11.5 to E15.5 showed disruption of column formation in both *Cdh2* and *Itgb1* mutants as compared with wild-type (Figure 2A; Supplemental Figure S4). Consistent with previous observations (Aszodi *et al.*, 2003), *Itgb1*-mutant chondrocytes exhibited more spherical shape as indicated by a smaller aspect ratio (AR = long axis/short axis) of proliferative chondrocytes compared with wild-type and *Cdh2*-mutant chondrocytes (Figure 2, B and C). No statistically significant difference between the genotypes was observed for chondrocyte perimeter, area, or curvature values at the time of initial cell division (Supplemental Figure S5). Collectively, these data validate the conditional genetic models used in the following studies.

In contrast to wild-type proliferative chondrocytes, both *Cdh2* and *Itgb1* mutants have defects in rotation, which was confirmed by long-term live tissue imaging (Figure 3, A–G; Supplemental Video S2 and S3; Supplemental Figure S4). Loss of *Itgb1* function showed greater effect on chondrocyte rotation compared with *Cdh2* mutants as measured by reduction in angle of rotation (Figure 3C) and frequent observation of misorientation of the initial division plane compared with wild-type and *Cdh2*-mutant cells (Supplemental Figure S6). Representative plots of single-cell trajectories for both *Cdh2* (Figure 3F) and *Itgb1* (Figure 3G) mutants generally show limited rotation of the division plane followed by a stable final orientation that was characterized by constant small fluctuations ("wobble") in position over time (compare with wild-type trajectories in Figure 3E). A subset of *Cdh2*- and *Itgb1*-mutant chondrocytes that undergo partial rotation events exhibit a novel trajectory phenotype in that the transition to termination of rotation is prolonged, resulting in a curve (Figures 3F and 5I) rather than the sharp transition observed in wild-type chondrocytes (Figures 3E and 5I). A subset of daughter cell pairs in both mutant groups displayed an increase in distance between neighboring cell membranes at the edges of the cell–cell interface, described as a constricting or pinching behavior (see magnified image of *Cdh2* mutant in Figure 3B and Supplemental Figure S4). This pinching phenotype occurs more frequently in *Itgb1* and *Cdh2* mutants compared with wild-type proliferative chondrocytes (Figure 3, H). *Itgb1* mutants and, to a lesser degree, *Cdh2* mutants also exhibit reduced time to pinching compared with wild type, potentially a result of impaired adhesion or cytoskeletal dynamics in the cell (Figure 3, I and J).

Epistatic relationship between *Cdh2* and *Itgb1*

The apparent requirement for both N-cadherin and β1 integrin suggests a potential reciprocal regulatory interaction between the two adhesion surfaces. To test this hypothesis, we analyzed phenotypes of an allelic series by breeding the *Cdh2*- and *Itgb1*-mutant mouse models together. We started by comparing zonal architecture in the allelic series, specifically focused on column architecture of the proliferative zone. We observed that *Itgb1*-mutant chondrocytes show defects in column structure regardless of the *Cdh2* genotype, as expected from the single mutation studies (Figure 4A). Surprisingly, chondrocytes mutant for *Cdh2* and heterozygous for *Itgb1* are phenotypically wild type with organized columns (Figure 4A). PCR analysis confirmed efficient recombination of conditional alleles in the *Cdh2*$^{-/-}$, *Itgb1*$^{-/-}$, *Cdh2*$^{-/-}$;*Itgb1*$^{-/-}$, *and Cdh2*$^{-/-}$;*Itgb1*$^{+/-}$ genotypes using validated primer sets (Figure 4, B and C; Supplemental Figure S7) (Kostetskii *et al.*, 2005; Chan *et al.*, 2006). We confirmed using long-term live tissue imaging that *Cdh2*$^{-/-}$;*Itgb1*$^{+/-}$ proliferative chondrocytes have normal cell division and rotation behaviors (Figure 5, A–C; Supplemental Video S4; Supplemental Figure S8). There is a strong initial division plane angle bias toward 0, and the final division plane angle has a bimodal distribution toward +90° or –90° (Figure 5B). Other measures of cell parameters largely confirmed wild-type cell behaviors using cell rotation angle (Figure 5C), aspect ratio (Figure 5D), and pinching behavior (Figure 5, E and F). Despite the overall wild-type appearance of proliferative

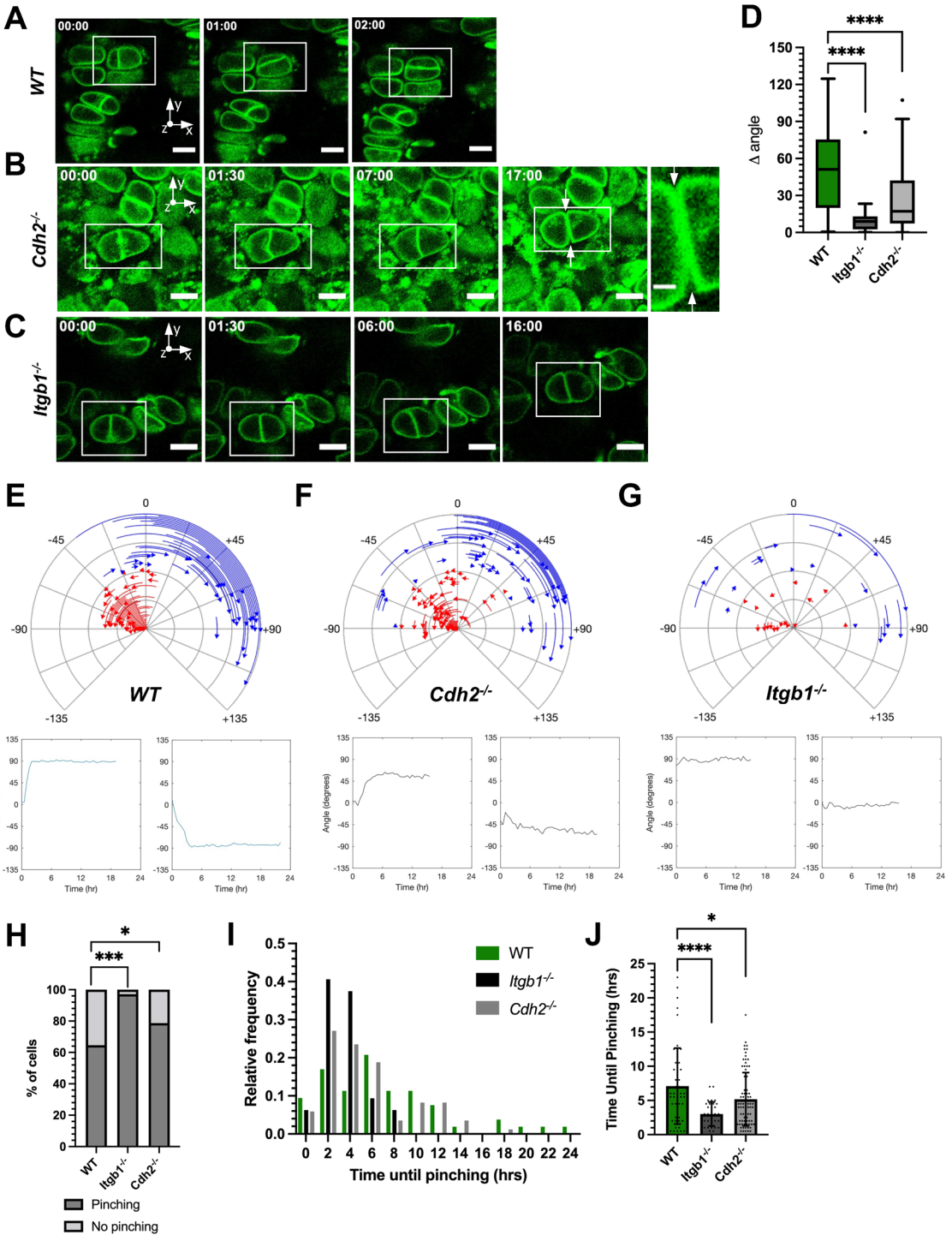

FIGURE 3: Rotation defect with loss of N-cadherin and β1 integrin. (A–C) Time-lapse frames of wild-type (A), *Cdh2*-mutant (B) and *Itgb1*-mutant (C) proliferative chondrocytes identify a failure of rotation. Arrow indicates a pinching away of the daughter cell membranes at the interface with the extracellular matrix domain. Magnified view shown at end of (B) with scale bar representing 2.5 μm. Panel (A) is replicated from Figure 1. (D) Shorter change in angle in *Itgb1*- and *Cdh2*-mutant cells compared with WT. (E–G) Angular trajectories for each dividing cell starting with the initial division plane angle and projecting towards the final rotation angle (arrowhead). Representative plots of single-cell trajectories shown below. Panel E is replicated from Figure 1. (H–J) Premature pinching phenotype for daughter cells where the cell-cell interface meets the cell-matrix junction (arrows in A). The percentage of cells pinching in the imaging period (H) and the frequency distribution of the time until pinching occurs with a bin size of 2 (I). (J) There is premature daughter cell pinching in the *Itgb1* and *Cdh2* mutants compared with WT. *N* (*Cdh2*) = 108 cells from 7 mice. *N* (*Itgb1*) = 35 cells from 4 mice. *N* (WT) = 82 cells from 10 mice. Comparisons of distributions of each mutant to the WT group performed using a two-tailed Kolmogorov–Smirnov test in panels (D) and (J). Comparisons of each mutant to the WT group performed using the Fisher's exact test for comparisons in (H). *$p < 0.05$, ***$p < 0.001$, ****$p < 0.0001$. Scale bar represents 10 μm.

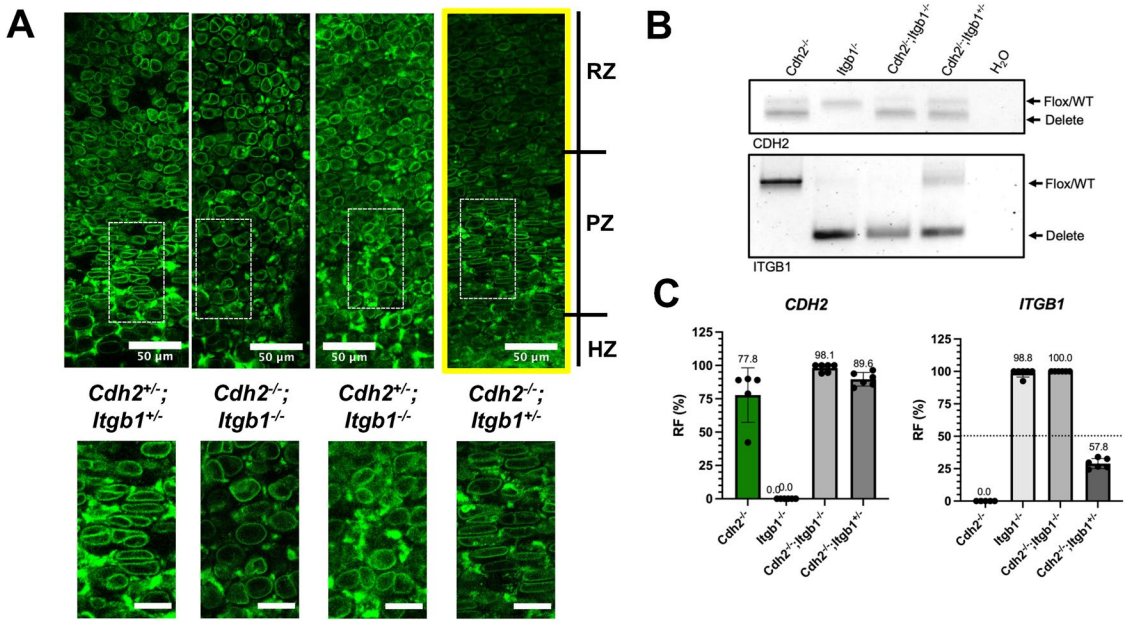

FIGURE 4: Compound mutants identify *Cdh2*$^{-/-}$;*Itgb1*$^{+/-}$ to rescue wild-type growth plate zonal architecture. (A) Allelic series of *Cdh2* and *Itgb1* compound mutations to identify potential genetic interactions. Failure to form aligned clonal columns in proliferative zone of *Cdh2*$^{-/-}$;*Itgb1*$^{-/-}$ and *Cdh2*$^{+/-}$;*Itgb1*$^{-/-}$ cranial bases compared with normal aligned columns in the *Cdh2*$^{+/-}$;*Itgb1*$^{+/-}$ and *Cdh2*$^{-/-}$;*Itgb1*$^{+/-}$ (yellow outline) groups. Magnification of dashed box region included below respective genotype. (B) Representative DNA gel of cartilage-specific recombination of respective samples following PCR amplification designed to produce differentially sized PCR products. (C) Quantification of band intensities (like those in B) expressed as recombination frequency (RF) (delete*100/delete + flox) for both *CDH2* and *ITGB1* genes. Dashed line represents what would be 100% recombination of the floxed allele in a heterozygote. *N* = 5–6 mice. Scale bar represents 20 µm, unless otherwise noted.

chondrocyte columns (Figure 4A), trajectory analysis (Figure 5B) revealed slower transition to terminate rotation and the distinct "wobble" of the cell interface postrotation, demonstrating that heterozygosity for *Itgb1* does not rescue all aspects of the *Cdh2*-mutant phenotype. Together, these findings demonstrate that *Itgb1* is epistatic to *Cdh2* and support the concept that proper balance in adhesion strength at different surfaces is essential for rearrangement of proliferative chondrocytes into columns.

To further define the relationship between *Cdh2* and *Itgb1* function, we analyzed gene expression using RT-qPCR of *Itgb1* and *Cdh2* in hind limb growth plate cartilage in the single mutations of *Cdh2*$^{-/-}$ and *Itgb1*$^{-/-}$, the phenotypically wild-type *Cdh2*$^{-/-}$;*Itgb1*$^{+/-}$, and true genetic wild-type embryos. Either single mutant shows reduced expression of the respective deleted genes, although *Itgb1* expression in *Cdh2* mutants trended toward a slight increase (not statistically significant). By contrast, *Cdh2*$^{-/-}$;*Itgb1*$^{+/-}$ embryos displayed reduced expression of *Cdh2* and nearly 50% reduction in *Itgb1*, which restores *Itgb1* expression to near normal levels, as compared with *Cdh2* mutants (Figure 5, G and H).

DISCUSSION

Proliferative chondrocyte rotation is a process that is of major importance during endochondral ossification of growth plate cartilage as the resulting columns aligned with the primary growth vector of the bone might potentiate effects of chondrocyte hypertrophy and matrix mineralization on bone growth. Previous studies by our lab and others described requirement for cadherin-mediated cell–cell adhesion in proliferative chondrocyte rearrangement and column formation. The current work extends these studies by elucidating roles for both cell–cell and cell–matrix adhesion and providing evidence for cross-talk of N-cadherin and β1 integrin during column formation (Figure 6).

New software extends quantitative analysis of dynamic chondrocyte cell behaviors

As previously demonstrated, our time-lapse imaging platform allows for novel observations of dynamic cell behaviors that underlie the generation of growth plate zonal architecture. However, the manual approaches to image segmentation and measurement practically limited the analysis to initial and final time points to study rearrangement and calculation of the aspect ratio from estimation of the short and long axes of the cell. Using B-splines to more easily and accurately captured geometric data over time enables measurement of more variables that increases confidence when comparing phenotypes. Additionally, we included automated ability to blind investigators during the analysis to maintain the highest standards of rigor and reproducibility in image analysis. Although this software represents a substantial step forward, some measurements retain subjective components, such as the need to manually mark the start of division, initiation of pinching, and the time point for separation of daughter cells. Ultimately, representative plots of single-cell division plane trajectories over time (all trajectories reported in Figure 5I), and other additional measures, will help stratify mutant phenotypes into distinct groups that may uncover potential gene interactions not predicted from known pathway architecture. Overall, the new software has generally improved efficiency and resolution over previous manual methods and provides a path to develop larger databases that enable finer resolution of phenotypes.

Inducible genetic murine models are reproducible and exhibit efficient recombination

One challenge to performing analysis of early skeletal development is the need for inducible genetic systems to avoid potential confounding effects of mutations on patterning and establishment of

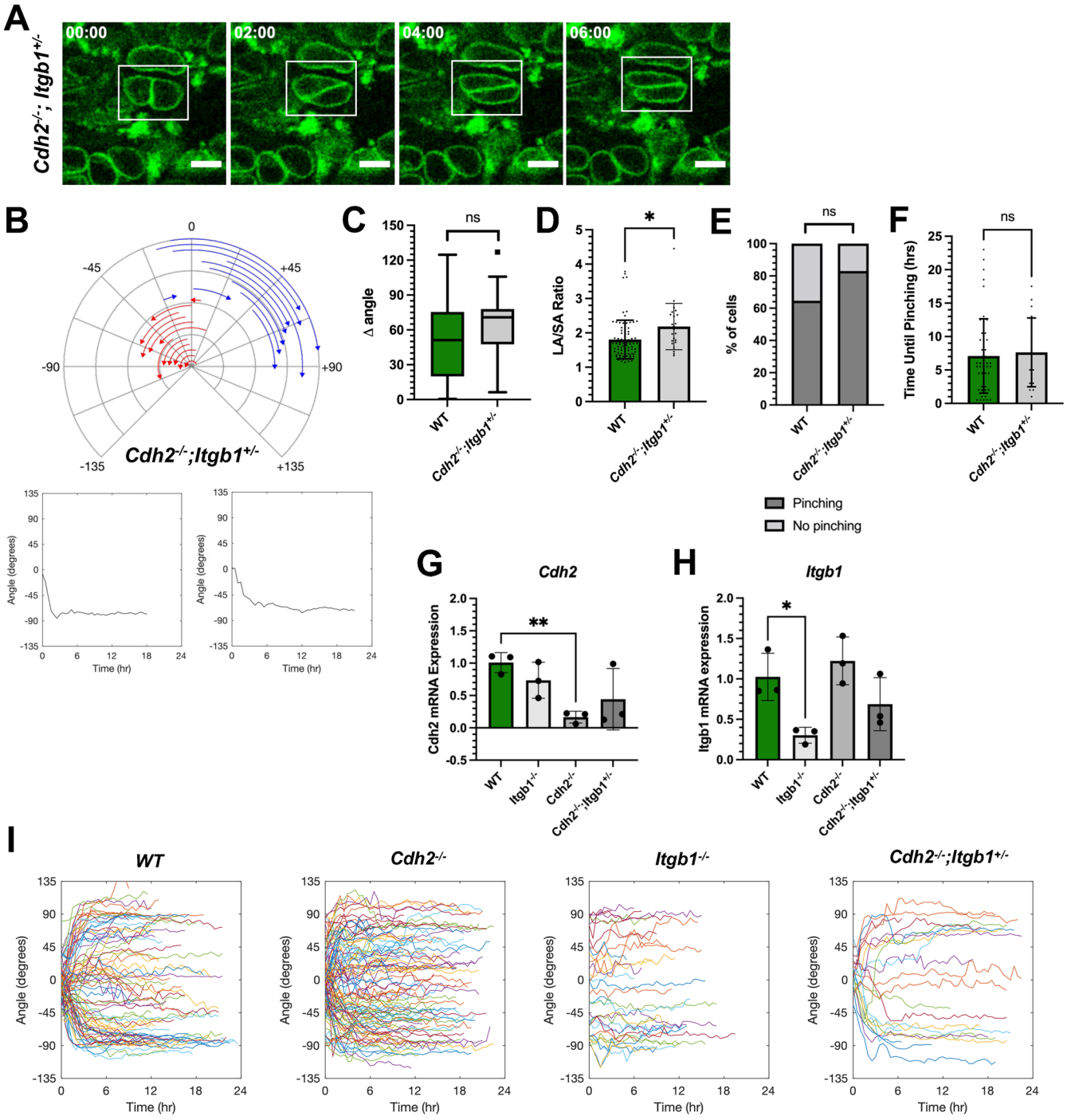

FIGURE 5: *Cdh2*$^{-/-}$;*Itgb1*$^{+/-}$ rescues many aspects of the wild-type proliferative chondrocyte phenotype. (A) Time-lapse frames of *Cdh2*$^{-/-}$;*Itgb1*$^{+/-}$ mutant proliferative chondrocyte undergoing ~ 90-degree rearrangement. (B) Angular trajectories for each dividing cell starting with the initial division plane angle and projecting toward final rotation angle. Representative plots of single-cell trajectories shown below. *N* = 23 cells from 4 mice. Comparison of change in angle (C), long axis to short axis aspect ratio (D), frequency of cell pinching phenotype (E), and time until daughter cell pinching (F) between *Cdh2*$^{-/-}$;*Itgb1*$^{+/-}$ and WT groups. (G–H) Gene expression analysis of *Itgb1*$^{-/-}$, *Cdh2*$^{-/-}$, and *Cdh2*$^{-/-}$;*Itgb1*$^{+/-}$ hindlimb growth plate cartilage as compared with WT using RT-qPCR to compare gene expression of *Cdh2* (G) and *Itgb1* (H). Values are expressed as ΔΔCt ± SD. *N* = 3 for each genotype. Each *N* is isolated from 5–10 embryonic day 17.5 pups. (I) Composite cell trajectory plots for all cells imaged for each genotype. *N* values are provided in this and earlier figures. Scale bar represents 10 μm unless otherwise indicated. Comparison of distributions between groups using Kolmogorov–Smirnov test in (C), (D), and (F). Comparison between mutant groups and WT using Fisher's exact test in (E) and using a Welch's *t* test in (G) and (H). *$p < 0.05$, **$p < 0.01$. ns = not significant.

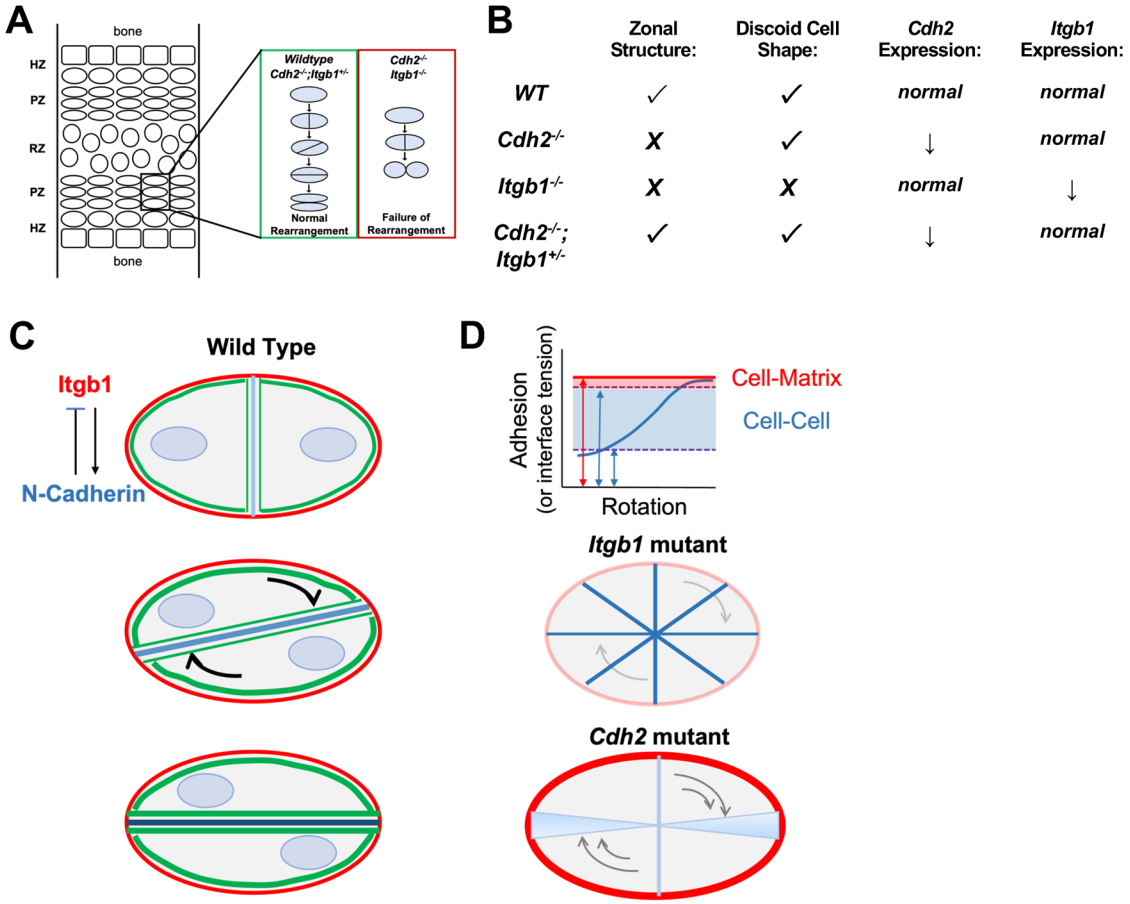

FIGURE 6: Summary and proposed model of balanced cell adhesion surface activity. (A) *Cdh2*$^{-/-}$;*Itgb1*$^{+/-}$ rescues wild-type proliferative daughter cell rearrangement behavior, while single mutants of *Cdh2*$^{-/-}$ and *Itgb1*$^{-/-}$ fail to assemble daughter cells into columns aligned with the primary growth direction of the bone. (B) Summary of how each genotype affects zonal structure, cell shape, *Cdh2* expression, and *Itgb1* expression. (C) A proposed model for regulation of daughter cell rearrangement by the coordinated action of cell–cell (via N-cadherin, blue) and cell-matrix (via β1 integrin, red) adhesion surfaces, potentially involving actomyosin tension (green). Following cell division and establishment of the cell–cell adhesion surface, we propose that integrin β1 drives cell rearrangement via imparting traction forces on the matrix and promoting cadherin adhesion to increase the cell–cell adhesion surface area. Cell rotation is complete when cell-cell adhesion or tension reaches a threshold that balances integrin-mediated forces. (D) A graphical summary of the model showing constant levels of cell–matrix adhesion with increasing levels of cell–cell adhesion during rotation. In wild-type cells, a narrow range of cell–matrix adhesion combined with a broader range of cell–cell adhesion is required for cell rearrangement. The lines with double arrowheads show the range of cell–cell to cell–matrix adhesion ratios that are permissive for cell rearrangement. Rounder cell shape and arbitrary division plane position in *Itgb1* mutants show that cell–matrix adhesion defines cell shape and orients the mitotic spindle. Loss of cell rearrangement in *Itgb1* mutants could result directly from reduced traction forces or indirectly via failure to promote growth of the cell–cell adhesion surface. In *Cdh2* mutants, deficiency in N-cadherin leads to reduced cell–cell adhesion and increased cell–matrix adhesion, which together result in an adhesion ratio that falls near or beyond the threshold for cell rearrangement, which results in variable rotation (different size arrows) and lack of a sharp transition at the end of rearrangement (graded triangles).

the cartilage template. Although recombination of *loxP* sites by tamoxifen-inducible *cre* recombinase activity is a well-established approach in mouse genetics, variable recombination frequencies of different conditional loci are a caveat that potentially makes estimates of recombination frequency unreliable when calculated using reporter alleles. These potential issues are compounded when multiple conditional alleles must be quantitatively recombined to limit phenotype variability, which is essential to support rigorous analysis and interpretation. In both single conditional mutants and the allelic series to screen compound mutants of *Cdh2* and *Itgb1*, each genotype expressed a consistent morphological phenotype observed in fluorescence images from over ten independent experiments using different combinations of parental genotypes. The prediction of high recombination frequency suggested by consistent phenotypes was strongly supported by PCR-based recombination analysis using validated primers (Kostetskii *et al.*, 2005; Chan *et al.*, 2006) that yielded calculated efficiencies of 75%–100% for all alleles and allelic combinations. Despite these high recombination frequencies, at least a few wild-type–like rotations were observed for every genotype. It remains uncertain whether these wild-type cell behaviors reflect the proportion of cells in which *loxP* recombination was incomplete or the deleted gene products had not sufficiently decayed. Alternatively, wild-type–like movements could suggest incomplete penetrance of the phenotype at the cellular level as has

been shown with planar cell polarity signaling (Etheridge *et al.*, 2008; Ahrens *et al.*, 2009). Unfortunately, the current methods for determining recombination analysis do not provide the single-cell resolution needed to test these proposed mechanisms.

β1 integrin drives chondrocyte rotation

Previous studies by our lab and as confirmed by others demonstrated requirement for cadherin adhesion for chondrocyte rearrangement and column formation. Although this conclusion was supported by results in different systems using distinct inhibitors of cadherin adhesion, the nonspecific actions of some reagents and the potential for off-target effects of others present several caveats to the prevailing model. Similar to our inhibitor studies, conditional deletion of *Cdh2* results in normal placement of the division plane and initiation of cell rotation that progresses to similar extent in both genetic and non-genetic inhibitor studies. What remains unclear is whether the partial rearrangements we observe relate to incomplete inhibition of N-cadherin activity (e.g., incomplete degradation of cell surface N-cadherin in mutant cells) (Romereim *et al.*, 2014) or whether the lack of rearrangement observed by Li *et al.* (Li *et al.*, 2017) results from off-target effects (e.g. other cadherins or interference with N-cadherin function in condensing mesenchyme). Despite extensive corroborating evidence favoring requirement for N-cadherin, the wild-type phenotype of *Cdh2*$^{-/-}$;*Itgb1*$^{+/-}$ proliferative chondrocytes demonstrates that N-cadherin is not essential for column formation. Rather, the observations of a consistent phenotype in *Itgb1* mutants regardless of the *Cdh2* genotype, greater effect of loss of *Itgb1* on rearrangement, reduced variability in phenotype expressivity, and more significant cell shape change all converge at the central role for *Itgb1* in the mechanism of rearrangement. These observations in the growth plate mirror requirement for both N-cadherin and β1 integrin in the mesenchymal cell to chondrocyte differentiation process, and a role for β1 integrin in creating structural organization and maintaining cell shape in conditional deletions of β1 integrin both in early limb mesenchyme (*Prrx1-cre*) and cartilage (*Col2a1-cre*) (DeLise & Tuan, 2002; Aszodi *et al.*, 2003; Raducanu *et al.*, 2009; Bougault *et al.*, 2013;).

Proper levels of cell adhesion are essential for chondrocyte rotation

Rescue of chondrocyte rearrangement in *Cdh2* mutants by heterozygous loss of *Itgb1* function is consistent with the requirement for balance in levels of adhesion at both the cell–cell and cell–matrix interfaces. A recent report showing defects in chondrocyte rotation in long bones deficient in α-parvin, a component of the focal adhesion complex, supports the importance of *Itgb1* activity levels in growth plate development (Yuan *et al.*, 2023). Studies in enteric nervous system (ENS) development have demonstrated a similar cooperative interaction between β1 integrin and N-cadherin (Broders-Bondon *et al.*, 2012). Deletion of N-cadherin in enteric neural crest cells rescues the neuronal organization and distribution of β1 integrin–depleted cells, consistent with a model in which loss of N-cadherin modifies the balance between cell–cell and cell–matrix adhesion. Likewise, β1 integrin–depleted cells have reduced cell–matrix adhesion and changes the overall adhesion balance in favor of intercellular adhesion (Monier-Gavelle & Duband, 1997). Simultaneous reduction in intercellular adhesion and ECM adhesion in double mutant enteric neural crest cells restores the balance between the two adhesion surfaces (despite reduction in total adhesion compared with controls), which results in normal neural network organization but fails to rescue migration defects. Analogously, cell trajectories demonstrate deficiencies in the rotation process that are consistent with the *Cdh2*-mutant phenotype, even though chondrocyte rotation is rescued by reestablishing balance between the cell adhesion surfaces. Specifically, the general absence of a sharp transition at the conclusion of rotation and presence of "wobble" of the daughter cell interface following cessation of rotation suggests that absolute levels of cell adhesion may be necessary to generate a robust braking mechanism that stabilizes final daughter cell position (Figure 6C).

Coordinated function of the cell–cell and cell–matrix adhesion surfaces was also evident in the constriction (pinching) phenomenon at the margins of the cell–cell interface that preceded separation of daughter cells. Loss of *Itgb1* function greatly increased the frequency of pinching while decreasing the time interval from establishment of the division plane to initiation of pinching. One possible interpretation is that deletion of *Itgb1* enhances cadherin adhesion and interfacial tension to accelerate pinching at the daughter cell interface. In this model, the greater proportion of cell pairs exhibiting pinching might reflect delayed daughter cell separation resulting from stabilization of the cell–cell adhesion surface or reduced cell–matrix tension needed to pull cell pairs apart. Paradoxically, we noted that deletion of *Cdh2* also increased the frequency of cell pinching (though to a lesser degree) but did not appreciably reduce time to pinching. A similar pinching phenotype was also previously observed by transmission electron microscopy following treatment with inhibitors of cadherin adhesion (Romereim *et al.*, 2014). One solution to this paradox is if time to pinching is a cadherin-dependent event that is antagonized (delayed in execution) by *Itgb1* function. In this case, reduction in N-cadherin with concomitant maintenance of β1 integrin could generate normal pinching times and the increase in pinching frequency in *Cdh2* mutants could reflect β1 integrin–dependent stabilization of the cell–cell interface via activation of alternative cadherins. Regardless, collectively, these data demonstrate that balance coordinated regulation of cell–cell and cell–matrix adhesion is essential at multiple steps in the generation of chondrocyte columns.

Although our data suggest the possibility of transcriptional regulation in balancing the activity of cell adhesion surfaces, it remains possible that these relatively small differences reflect long-term adaptations of the system (as measured six days after initial recombination) rather than direct regulatory mechanisms. Other mechanisms may also regulate feedback between the two adhesion surfaces. Many studies in other systems support the existence of crosstalk between cadherins and integrins to regulate cell behavior in a cell-specific and environment-specific context (Gimond *et al.*, 1999; Marsden & DeSimone, 2003; Yano *et al.*, 2004; de Rooij *et al.*, 2005; Huttenlocher & Horwitz, 2011; Quadri, 2012; Mui *et al.*, 2016; Barcelona-Estaje *et al.*, 2021; Zhang *et al.*, 2022). Cell–ECM contacts and intercellular junctions share signaling molecules, yet some execute site-specific mechanical roles depending on their localization and discrete posttranslational modifications, like with vinculin and cofilin (Bays *et al.*, 2014; Auernheimer *et al.*, 2015; Zhang *et al.*, 2022). Integrin-based adhesions and cadherin-dependent junctions experience matrix stiffness and external mechanical forces and the variations in adhesion strength across the cell can generate shifts in the balance of tension across both adhesion systems. This is a type of tensional homeostasis, which is important for organizing and localizing adhesion within cells. Several studies have demonstrated that strengthening of adhesion at one surface opposes tension at the other. For example, it was shown that strong ECM-integrin engagement leads to downstream FAK activation resulting in a loss of N-cadherin–mediated intercellular contacts (Yano *et al.*, 2004). Interactions between the cell–cell and cell–matrix adhesions are not

specifically antagonistic but can also be cooperative and interdependent to allow the cell to achieve tensional homeostasis (Mui *et al.*, 2016; Howden *et al.*, 2021; Hadjisavva *et al.*, 2022).

A model for initiation of column formation

These reported observations also provide a foundation for understanding the mechanism that generates cellular organization in the resting zone and makes specific predictions about the transition to column formation. Although our current studies appear agnostic with respect to whether too much or too little cell adhesion prevents chondrocyte rotation in the resting zone, the rounder shape of resting chondrocytes (as with *Itgb1*$^{-/-}$ chondrocytes) is highly suggestive of reduced adhesion at the cell–ECM surface. An additional consequence of reduced ECM adhesion is misplacement of the cell division plane, as the rounder shape could impact spindle alignment to the long axis of the cell (Hertwig's rule) (Wilson, 1900; Dodds, 1930). Thus, low integrin–ECM adhesion could result in arbitrary planes of cell division and lack of daughter cell rearrangement that together would generate the "disorganization" of resting chondrocytes. Activation of cell rotation precedes cell shape changes in the transition to columnar cell arrangement (Romereim *et al.*, 2014), which is consistent with upregulation of *Itgb1* function by signaling pathways at the transition followed by matrix remodeling to promote cell shape change to align cell axes. However, the prediction of increased *Itgb1* expression in proliferative chondrocytes was not supported by RNA-sequencing studies (Lui *et al.*, 2018), although these data cannot rule out the potential for integrin activation via inside-out signaling. One intriguing possibility is that Gli3 directly or indirectly controls the switch mechanism since column formation was restored in *Ihh* mutants following deletion of *Gli3* (Hilton *et al.*, 2005).

MATERIALS AND METHODS

Request a protocol through *Bio-protocol*.

Materials

Unless otherwise indicated, chemicals and reagents are obtained from Sigma-Aldrich (St. Louis, MO) or Thermo Fisher Scientific (Waltham, MA); cell culture media from Life Technologies/Life Technologies (Grand Island, NY); oligonucleotides from IDT (Coralville, IA); consumables from Thermo Fisher Scientific or VWR (Radnor, PA); and confocal microscope and software from Carl Zeiss AG (Oberkochen, Germany).

Mouse genetics and tamoxifen injections

For all matings, embryonic day (E) 0.5 was designated as noon on the day of the postcoital plug. For live-cell imaging and phenotype analysis of the allelic series, female mice homozygous for the reporter allele [Gt(ROSA)26Sortm4(ACTB-tdTomato,-EGFP)Luo/J; Jackson Laboratories; stock #007576] were first mated with homozygous col2a1::creER^{T} males [FVB-Tg (Col2a1-cre/ERT)KA3Smac/J; Jackson Laboratories] (Muzumdar *et al.*, 2007). Subsequent crosses of the F1 generation were performed until males were homozygous for the tdTomato-eGFP reporter allele and homozygous for col2a1::creER^{T}, designated CTD males (see Table 1). The floxed Cdh2 line [B6.129S6(SJL)-Cdh2^{tm1Glr}/J; Jackson Laboratories; stock #007611] and floxed integrin B1 line [B6;129-Itgb1^{tm1Efu}/J; Jackson Laboratories; stock #004605] have been described previously (Kostetskii *et al.*, 2005; Raghavan *et al.*, 2000). Homozygous floxed females were bred with CTD males to ultimately generate homozygous floxed males with CTD. Pregnant females were injected daily intraperitoneally from E11.5- E15.5 with a 100 mg/kg dose of tamoxifen (20 mg/ml tamoxifen in 90% corn oil, 10% ethanol) to generate a pulse of cre activity and induce recombination in the floxed alleles, as well as to switch reporter allele expression from myristolated tdTomato to myristoylated eGFP (Lizen *et al.*, 2015). All procedures were consistent with regulatory agency policies and were approved by the Institutional Care and Use Committee at the University of Nebraska Medical Center.

Histology and Immunofluorescence

On embryonic day E15.5, cranial base growth plates were harvested, fixed in 4% paraformaldehyde in TBS overnight at 4°C, treated with 5 mg/ml sodium borohydride (Sigma-Aldrich), washed with PBS, and embedded for cryosection using OCT (Sakura Finetek USA, Torrance, CA) as previously described (Ahrens & Dudley, 2011). Tissue sections of 14 µm were used for histology. Immunofluorescence was performed as described, with the following pretreatments: autofluorescence quenching in 0.25% ammonia/70% ethanol for one hour; 2 mg/ml hyaluronidase in 100 mM NaCl, 10 mM sodium acetate, pH 5.6, 0.1% Triton X-100 at 37°C for 30 min; antigen retrieval in boiling 10 mM sodium citrate; and permeabilization in 0.5% Triton X-100/TBS for 20 min. Prior to blocking in 10% HISS for 2 h, the slides to be treated with mouse anti-N-cadherin primary antibody were treated with M.O.M. mouse IgG blocking reagent (Vector Laboratories, Burlingame, CA) for 1 h. Primary antibody for N-cadherin (1:50, Cell Signaling Technology, 14215S) was diluted in M.O.M. diluent and primary antibody for integrin β1 (1:50, Millipore Sigma, MABT821) was diluted in 2% HISS in TBST. Secondary antibody was diluted using the same respective diluents at a ratio of 1:100 using the following antibodies: donkey anti-mouse Cy3 (Jackson ImmunoResearch, West Grove, PA) and donkey anti-rat Cy3 (Jackson ImmunoResearch). Slides were mounted in VectaShield Antifade Mounting Medium with DAPI and sealed prior to confocal imaging at 40× using the tile scan function to capture the entire growth plate structure.

Recombination frequency analysis

Previously designed primers and PCR were utilized to assess recombination of the *CDH2* and *ITGB1* genes. DNA was isolated from E17.5 murine distal femur and proximal tibia growth plate cartilage using the salting-out method (Miller *et al.*, 1988) and resuspended in water. Oligonucleotide primers were used to distinguish the recombined Cdh2 allele from the unrecombined Cdh2$^{fl/fl}$ genotype by size and band intensity (Kostetskii *et al.*, 2005) and were obtained with conditions: 94°C 20 s, 61°C 15 s, and 72°C 10 s for 30 cycles. Oligonucleotide primers were used to distinguish the recombined Itgb1 allele from the unrecombined Itgb1$^{fl/fl}$ genotype by size (Raghavan *et al.*, 2000; Chan *et al.*, 2006) and were obtained with conditions: 94°C 20 s, 61°C 15 s, and 72°C 60 s for 30 cycles. Primer sequences are included in Table 2. PCR products were visualized using ethidium bromide after being loaded onto a 4% agarose gel, separated by electrophoresis at 100V for 1 h, and visualized under ultraviolet light. Measurement of band intensity was completed with ImageJ software (Fiji) using the gel analysis feature to plot band intensities. Recombination frequency was calculated using band intensities using the following equation: (delete × 100)/(delete + flox).

Explant cultures

Pregnant females with embryos at embryonic day 17.5 were euthanized and the cranial base growth plate cartilage, including a small amount of adjacent bone, were rapidly harvested into Hank's Balanced Salt Solution (HBSS) with magnesium and calcium and without phenol red (Life Technologies/Life Technologies). Cartilage explants were maintained briefly in a passively humidified incubator at

Mating schematic to develop cartilage-specific double fluorescence reporter model				
Female		**Male**	**F1 Generation**	**Abbreviation:**
$(mT/mG)^{+/+}$	x	Col2a1-creERT$^{+/+}$	$(mT/mG)^{+/-}$;Col2a1-creERT$^{+/-}$	
F1	x	F1	$(mT/mG)^{+/+}$;Col2a1-creERT$^{+/+}$	CTD
Mating schematic to develop inducible cartilage knockout with reporter of Cdh2:				
Female		**Male**	**F1 Generation:**	**With tamoxifen:**
CTD	x	Cdh2$^{fl/fl}$	Cdh2$^{fl/+}$;$(mT/mG)^{+/-}$;Col2a1-creERT$^{+/-}$	
F1	x	F1	Cdh2$^{fl/fl}$;$(mT/mG)^{+/+}$;Col2a1-creERT$^{+/+}$	Cdh2$^{-/-}$
Mating schematic to develop inducible cartilage knockout with reporter of Itgb1:				
Female		**Male**	**F1 Generation:**	**With Tamoxifen:**
CTD	x	Itgb1$^{fl/fl}$	Itgb1$^{fl/+}$;$(mT/mG)^{+/-}$;Col2a1-creERT$^{+/-}$	
F1	x	F1	Itgb1$^{fl/fl}$;$(mT/mG)^{+/+}$;Col2a1-creERT$^{+/+}$	Itgb1$^{-/-}$
Mating schematic to develop double mutants of Cdh2 and Itgb1:				
Female		**Male**	**F1 Generation:**	**With Tamoxifen:**
Cdh2$^{fl/fl}$	x	Itgb1$^{fl/fl}$;$(mT/mG)^{+/+}$;Col2a1-creERT$^{+/+}$	Cdh2$^{fl/+}$;Itgb1$^{fl/+}$;$(mT/mG)^{+/-}$;Col2a1-creERT$^{+/-}$	
F1	x	F1	Cdh2$^{fl/fl}$;Itgb1$^{fl/fl}$;$(mT/mG)^{+/+}$;Col2a1-creERT$^{+/+}$	Cdh2$^{-/-}$;Itgb1$^{-/-}$
Mating schematic for double mutant live imaging and RT-qPCR experiments:				
Female		**Male**	**F1 Generation:**	**With Tamoxifen:**
Cdh2$^{fl/fl}$	x	Cdh2$^{fl/fl}$;Itgb1$^{fl/fl}$;$(mT/mG)^{+/+}$;Col2a1-creERT$^{+/+}$	Cdh2$^{fl/fl}$;Itgb1$^{fl/+}$;$(mT/mG)^{+/-}$;Col2a1-creERT$^{+/-}$	Cdh2$^{-/-}$;Itgb1$^{+/-}$
Itgb1$^{fl/fl}$	x	Cdh2$^{fl/fl}$;Itgb1$^{fl/fl}$;$(mT/mG)^{+/+}$;Col2a1-creERT$^{+/+}$	Cdh2$^{fl/+}$;Itgb1$^{fl/fl}$;$(mT/mG)^{+/-}$;Col2a1-creERT$^{+/-}$	Cdh2$^{+/-}$;Itgb1$^{-/-}$
Cdh2$^{fl/fl}$;Itgb1$^{fl/fl}$	x	Cdh2$^{fl/fl}$;Itgb1$^{fl/fl}$;$(mT/mG)^{+/+}$;Col2a1-creERT$^{+/+}$	Cdh2$^{fl/fl}$;Itgb1$^{fl/fl}$;$(mT/mG)^{+/-}$;Col2a1-creERT$^{+/-}$	Cdh2$^{-/-}$;Itgb1$^{-/-}$

TABLE 1: Mouse genotypes and nomenclature.

37°C and 8% CO_2, then explants were placed on a LabTek 35 mm glass-bottom culture dish and embedded in 1% (wt/vol) SeaKem LE agarose (Lonza) in HBSS. After 5 min of gelation, 3 ml of cartilage culture media (MEM alpha medium without phenol red [Life Technologies] supplemented with 50 mg/ml penicillin–streptomycin [Life Technologies], L-Glutamine 100x [Life Technologies], 10 mM B-glycerophosphate [Sigma-Aldrich], 50 µg/ml L(+) ascorbic acid [Sigma-Aldrich], 1 nM dexamethasone [Sigma-Aldrich], 1 mg/ml proline [Thermo Fisher Scientific], 1% antioxidant [Sigma-Aldrich], 1 mM sodium pyruvate [Life Technologies], 1% nonessential amino acids [Sigma-Aldrich], and 1% Insulin–Transferrin–Selenium [Sigma-Aldrich]) was added into the dish.

Confocal live-tissue imaging set-up and image acquisition

Explant imaging was performed using a Zeiss 880 laser scanning confocal microscope equipped with a 37°C heated PeCon XLmutli S chamber and PeCon environmental control system (passive humidity, 8% CO_2). Every 30 min for up to 24 h, optical sections (line averaging of 8, scan speed of 10, and resolution of 1600 × 1600) captured eGFP-expressing chondrocytes at 2.0-µm intervals for a total depth of between 200 and 300 µm. One 336 µm x 336 µm viewing field was captured per cranial base toward the center on the posterior/caudal side of the intersphenoidal synchondrosis (ISS). The top of the hypertrophic zone, characterized by higher intensity of matrix vesicles and larger cell area, was used as a locational marker to make sure the adjacent proliferative zone was the primary zone included in the viewing field. Considering only the posterior/caudal end of the ISS, ~ 40–50% of the growth plate area was captured during each imaging session. Between four and ten growth plates were imaged for each genotype. The orientation of camera was adjusted so the growth direction of cranial base explant was parallel to the *y*-axis of the image.

Image processing and quantification

Zen Blue software (Zeiss) was used for postimage processing to identify dividing chondrocytes during the imaging period. An optical section, where the dividing cell was in-focus, was saved at each time point to later assemble z-stacks into movies of proliferating chondrocyte reconstructions using ImageJ software (Fiji). Cells were collected for each genotype. A custom written MATLAB program with graphical user interface was developed to facilitate the workflow of tracing and analyzing dividing cells under blinded conditions. In this integrated workflow, the user was presented with blinded image sets and traced the outer contour of the daughter cell

Gene		F sequence	R sequence	Reference
Itgb1	Distinguish by band size	CGCAGAACAATAGGTGCTGAAATTAC	CCACAACTTTCCCAGTTAGCTCTC	(Chan *et al.*, 2006; Raghavan *et al.*, 2000)
Cdh2	Deleted allele	TGCTGGTAGCATTCCTATGG	GTATGGCCAAGTAATGGGGAC	(Kostetskii *et al.*, 2005)
Cdh2	Floxed allele	TGCTGGTAGCATTCCTATGG	TACAAGTTTGGGTGACAAGC	(Kostetskii *et al.*, 2005)

TABLE 2: Primer sequences for recombination frequency analysis.

Gene	Accession Number	F sequence	R sequence	Product Size	Reference
Itgb1	NM_010578.2	AGACTTCCGCATTGGCTTTG	GCTGGTGCAGTTTTGTTCAC	112	(Piwko-Czuchra *et al.*, 2009)
Cdh2	NM_007664.5	TGAAACGGCGGGATAAAGAG	GGCTCCACAGTATCTGGTTG	157	(Guan *et al.*, 2014)
Actb	NM_007393.5	AAATCGTGCGTGACATCAAAGA	GCCATCTCCTGCTCGAAGTC	64	(Erickson *et al.*, 2018)
Hrpt	NM_013556.2	GACCTCTCGAAGTGTTGGATAC	TGCAGATTCAACTTGCGCTC	180	(Erickson *et al.*, 2018)
Rlp13a	NM_009438.5	ATCCCTCCACCCTATGACAA	GCCCCAGGTAAGCAAACTT	97	(Erickson *et al.*, 2018)

TABLE 3: Primer sequences for RT-qPCR.

membranes as well as the inner contour of the division plane using B-splines. The user also set checkboxes to indicated when division started, pinching occurred, and daughter cells separated. The saved B-spline data were then converted into polygons with 1024 evenly spaced points for final quantification of geometric variables within the indicated times. All plots were generated using either MATLAB or Prism software (GraphPad Software, Inc., La Jolla, CA).

Code availability

Image analysis code for tracing division plane of proliferative chondrocytes is available at: https://github.com/StephenHaller/CellTracer.

Phenotypic evaluation of allelic series

Tissue was fixed after harvesting with 4% paraformaldehyde (Sigma-Aldrich) in PBS. Confocal imaging set-up and image acquisition was the same as previously described. A z-stack of ~ 50–100 µm was taken at a single time point to capture the zonal architecture across the resting to hypertrophic zones (see Figure 1A).

RNA extraction and RT-qPCR

Total RNA from the growth plate at the base of the femur and head of the tibia of E17.5 embryos was prepared using the NucleoSpin RNA Plus kit (Thermo Fisher Scientific) according to the manufacturer's instructions. Articular cartilage and perichondrium were carefully removed using forceps. Growth plates were collected in HBSS and pulverized under liquid nitrogen before being added to the lysis buffer. Before isolating RNA using the kit, cartilage tissue was pulverized under liquid nitrogen, added to 350 µl of lysis buffer, aggravated on a rotating shaker for 45 min, and passed through a 22G syringe ten times to further homogenize the sample. To increase RNA elution during extraction, the same 40 µl of water was passed through the final column twice. RNA was quantified by using a Thermo Fisher Scientific NanoDropOne spectrophotometer. cDNA was synthesized by using Superscript IV (Thermo Fisher Scientific) according to the manufacturer's instructions. Quantitative PCR was performed using the QuantStudio 3 Real-Time PCR system (Applied Biosystems by Thermo Fisher Scientific) to measure the relative expression levels of N-cadherin (*Cdh2*) and β1 integrin (*Itgb1*) using the Absolute Blue qPCR SYBR Green ROX kit (Thermo Fisher Scientific) (see Tables 2 and 3). Samples were normalized with a geometric average of *Actb*, *RLP13a*, and *HPRT* expression. Data from this analysis are reported as ΔΔCt values ± SD, and significance was determined using Welch's *t* test in Prism software by comparing the mutant genotypes to wildtype. A full list of primer sequences, accession numbers, and product sizes used for qPCR are included in Supplemental Table S2.

Statistical analysis

Values were reported as mean ± SD. To determine if frequency distributions between the wild type and each mutant group were statistically significant, a two-tailed Kolmogorov–Smirnov test was used. Comparison between means of each mutant group to wild type for the gene expression data was performed using Welch's *t* test. Comparison of the categorical data for pinching frequency was performed using Fisher's exact test. Significance level of 0.05 was selected for statistical analysis.

ACKNOWLEDGMENTS

This study was supported by the Mary and Dick Holland Regenerative Medicine program, the Child Health Research Institute at the University of Nebraska Medical Center, and the National Institute of Arthritis, Musculoskeletal, and Skin Diseases (NIAMS/AR070242). The authors wish to thank the UNMC Comparative Medicine team for their technical assistance. The authors have no conflict of interest to declare.

REFERENCES

Abad V, Meyers JL, Weise M, Gafni RI, Barnes KM, Nilsson O, Bacher JD, Baron J (2002). The role of the resting zone in growth plate chondrogenesis. Endocrinology 143, 1851–1857.

Agirdil Y (2020). The growth plate: a physiologic overview. EFORT Open Rev 5, 498–507.

Ahrens MJ, Dudley AT (2011). Chemical pretreatment of growth plate cartilage increases immunofluorescence sensitivity. J Histochem Cytochem 59, 408–418.

Ahrens MJ, Li Y, Jiang H, Dudley AT (2009). Convergent extension movements in growth plate chondrocytes require gpi-anchored cell surface proteins. Development 136, 3463–3474.

Ahrens MJ, Romereim S, Dudley AT (2011). A re-evaluation of two key reagents for in vivo studies of Wnt signaling. Dev Dyn 240, 2060–2068.

Aszodi A, Hunziker EB, Brakebusch C, Fassler R (2003). Beta1 integrins regulate chondrocyte rotation, G1 progression, and cytokinesis. Genes Dev 17, 2465–2479.

Auernheimer V, Lautscham LA, Leidenberger M, Friedrich O, Kappes B, Fabry B, Goldmann WH (2015). Vinculin phosphorylation at residues Y100 and Y1065 is required for cellular force transmission. J Cell Sci 128, 3435–3443.

Barcelona-Estaje E, Dalby MJ, Cantini M, Salmeron-Sanchez M (2021). You Talking to Me? Cadherin and Integrin Crosstalk in Biomaterial Design. Adv Healthc Mater 10, e2002048.

Bays JL, Peng X, Tolbert CE, Guilluy C, Angell AE, Pan Y, Superfine R, Burridge K, DeMali KA (2014). Vinculin phosphorylation differentially regulates mechanotransduction at cell-cell and cell-matrix adhesions. J Cell Biol 205, 251–263.

Bougault C, Cueru L, Bariller J, Malbouyres M, Paumier A, Aszodi A, Berthier Y, Mallein-Gerin F, Trunfio-Sfarghiu AM (2013). Alteration of cartilage mechanical properties in absence of beta1 integrins revealed by rheometry and FRAP analyses. J Biomech 46, 1633–1640.

Broders-Bondon F, Paul-Gilloteaux P, Carlier C, Radice GL, Dufour S (2012). N-cadherin and beta1-integrins cooperate during the development of the enteric nervous system. Dev Biol 364, 178–191.

Chan CS, Weeber EJ, Zong L, Fuchs E, Sweatt JD, Davis RL (2006). Beta 1-integrins are required for hippocampal AMPA receptor-dependent synaptic transmission, synaptic plasticity, and working memory. J Neurosci 26, 223–232.

Chen L, Adar R, Yang X, Monsonego EO, Li C, Hauschka PV, Yayon A, Deng CX (1999). Gly369Cys mutation in mouse FGFR3 causes achondroplasia

by affecting both chondrogenesis and osteogenesis. J Clin Invest 104, 1517–1525.
de Rooij J, Kerstens A, Danuser G, Schwartz MA, Waterman-Storer CM (2005). Integrin-dependent actomyosin contraction regulates epithelial cell scattering. J Cell Biol 171, 153–164.
DeLise AM, Tuan RS (2002). Alterations in the spatiotemporal expression pattern and function of N-cadherin inhibit cellular condensation and chondrogenesis of limb mesenchymal cells in vitro. J Cell Biochem 87, 342–359.
Dodds GS (1930). Row formation and other types of arrangement of cartilage cells in endochondral ossification. The Anatomical Record 46, 385–399.
Etheridge SL, Ray S, Li S, Hamblet NS, Lijam N, Tsang M, Greer J, Kardos N, Wang J, Sussman DJ, *et al.* (2008). Murine dishevelled 3 functions in redundant pathways with dishevelled 1 and 2 in normal cardiac outflow tract, cochlea, and neural tube development. PLoS Genet 4, e1000259.
Feil R, Wagner J, Metzger D, Chambon P (1997). Regulation of Cre recombinase activity by mutated estrogen receptor ligand-binding domains. Biochem Biophys Res Commun 237, 752–757.
Gibson BG, Briggs MD (2016). The aggrecanopathies; an evolving phenotypic spectrum of human genetic skeletal diseases. Orphanet J Rare Dis 11, 86.
Gimond C, van Der Flier A, van Delft S, Brakebusch C, Kuikman I, Collard JG, Fassler R, Sonnenberg A (1999). Induction of cell scattering by expression of beta1 integrins in beta1-deficient epithelial cells requires activation of members of the rho family of GTPases and downregulation of cadherin and catenin function. J Cell Biol 147, 1325–1340.
Hadjisavva R, Anastasiou O, Ioannou PS, Zheltkova M, Skourides PA (2022). Adherens junctions stimulate and spatially guide integrin activation and extracellular matrix deposition. Cell Rep 40, 111091.
Hall BK, Miyake T (1992). The membranous skeleton: the role of cell condensations in vertebrate skeletogenesis. Anat Embryol (Berl) 186, 107–124.
Hall BK, Miyake T (2000). All for one and one for all: condensations and the initiation of skeletal development. Bioessays 22, 138–147.
Hallett SA, Matsushita Y, Ono W, Sakagami N, Mizuhashi K, Tokavanich N, Nagata M, Zhou A, Hirai T, Kronenberg HM, Ono N (2021). Chondrocytes in the resting zone of the growth plate are maintained in a Wnt-inhibitory environment. eLife 10, e64513.
Harrison RG (1924). Some Unexpected Results of the Heteroplastic Transplantation of Limbs. Proc Natl Acad Sci USA 10, 69–74.
Hilton MJ, Tu X, Cook J, Hu H, Long F (2005). Ihh controls cartilage development by antagonizing Gli3, but requires additional effectors to regulate osteoblast and vascular development. Development 132, 4339–4351.
Hirai T, Chagin AS, Kobayashi T, Mackem S, Kronenberg HM (2011). Parathyroid hormone/parathyroid hormone-related protein receptor signaling is required for maintenance of the growth plate in postnatal life. Proc Natl Acad Sci USA 108, 191–196.
Howden JD, Michael M, Hight-Warburton W, Parsons M (2021). α2β1 integrins spatially restrict Cdc42 activity to stabilise adherens junctions. BMC Biol 19, 130.
Hsieh YL, Wei X, Wang Y, Zhang H, Qi S, Xie D, Mishina Y, Mendonca D, Hatch N, Liu F (2021). Chondrocyte Tsc1 controls cranial base bone development by restraining the premature differentiation of synchondroses. Bone 153, 116142.
Hunziker EB (1994). Mechanism of longitudinal bone growth and its regulation by growth plate chondrocytes. Microsc Res Tech 28, 505–519.
Hunziker EB, Schenk RK (1989). Physiological mechanisms adopted by chondrocytes in regulating longitudinal bone growth in rats. J Physiol 414, 55–71.
Huttenlocher A, Horwitz AR (2011). Integrins in cell migration. Cold Spring Harb Perspect Biol 3, a005074.
Kember NF, Walker KV (1971). Control of bone growth in rats. Nature 229, 428–429.
Kostetskii I, Li J, Xiong Y, Zhou R, Ferrari VA, Patel VV, Molkentin JD, Radice GL (2005). Induced deletion of the N-cadherin gene in the heart leads to dissolution of the intercalated disc structure. Circ Res 96, 346–354.
Koyama E, Young B, Nagayama M, Shibukawa Y, Enomoto-Iwamoto M, Iwamoto M, Maeda Y, Lanske B, Song B, Serra R, Pacifici M (2007). Conditional Kif3a ablation causes abnormal hedgehog signaling topography, growth plate dysfunction, and excessive bone and cartilage formation during mouse skeletogenesis. Development 134, 2159–2169.
Kronenberg HM (2003). Developmental regulation of the growth plate. Nature 423, 332–336.
Li Y, Li A, Junge J, Bronner M (2017). Planar cell polarity signaling coordinates oriented cell division and cell rearrangement in clonally expanding growth plate cartilage. eLife 6, e23279.
Lizen B, Claus M, Jeannotte L, Rijli FM, Gofflot F (2015). Perinatal induction of Cre recombination with tamoxifen. Transgenic Res 24, 1065–1077.
Lui JC, Jee YH, Garrison P, Iben JR, Yue S, Ad M, Nguyen Q, Kikani B, Wakabayashi Y, Baron J (2018). Differential aging of growth plate cartilage underlies differences in bone length and thus helps determine skeletal proportions. PLoS Biol 16, e2005263.
Maeda Y, Nakamura E, Nguyen MT, Suva LJ, Swain FL, Razzaque MS, Mackem S, Lanske B (2007). Indian Hedgehog produced by postnatal chondrocytes is essential for maintaining a growth plate and trabecular bone. Proc Natl Acad Sci USA 104, 6382–6387.
Marsden M, DeSimone DW (2003). Integrin-ECM interactions regulate cadherin-dependent cell adhesion and are required for convergent extension in Xenopus. Curr Biol 13, 1182–1191.
McBratney-Owen B, Iseki S, Bamforth SD, Olsen BR, Morriss-Kay GM (2008). Development and tissue origins of the mammalian cranial base. Dev Biol 322, 121–132.
Miller SA, Dykes DD, Polesky HF (1988). A simple salting out procedure for extracting DNA from human nucleated cells. Nucleic Acids Res 16, 1215.
Mizuhashi K, Ono W, Matsushita Y, Sakagami N, Takahashi A, Saunders TL, Nagasawa T, Kronenberg HM, Ono N (2018). Resting zone of the growth plate houses a unique class of skeletal stem cells. Nature 563, 254–258.
Monier-Gavelle F, Duband JL (1997). Cross talk between adhesion molecules: control of N-cadherin activity by intracellular signals elicited by beta1 and beta3 integrins in migrating neural crest cells. J Cell Biol 137, 1663–1681.
Mui KL, Chen CS, Assoian RK (2016). The mechanical regulation of integrin-cadherin crosstalk organizes cells, signaling and forces. J Cell Sci 129, 1093–1100.
Muzumdar MD, Tasic B, Miyamichi K, Li L, Luo L (2007). A global double-fluorescent Cre reporter mouse. Genesis 45, 593–605.
Nagayama M, Iwamoto M, Hargett A, Kamiya N, Tamamura Y, Young B, Morrison T, Takeuchi H, Pacifici M, Enomoto-Iwamoto M, Koyama E (2008). Wnt/beta-catenin signaling regulates cranial base development and growth. J Dent Res 87, 244–249.
Nakamura E, Nguyen MT, Mackem S (2006). Kinetics of tamoxifen-regulated Cre activity in mice using a cartilage-specific CreER(T) to assay temporal activity windows along the proximodistal limb skeleton. Dev Dyn 235, 2603–2612.
Ono N, Ono W, Nagasawa T, Kronenberg HM (2014). A subset of chondrogenic cells provides early mesenchymal progenitors in growing bones. Nat Cell Biol 16, 1157–1167.
Quadri SK (2012). Cross talk between focal adhesion kinase and cadherins: role in regulating endothelial barrier function. Microvasc Res 83, 3–11.
Raducanu A, Hunziker EB, Drosse I, Aszodi A (2009). Beta1 integrin deficiency results in multiple abnormalities of the knee joint. J Biol Chem 284, 23780–23792.
Raghavan S, Bauer C, Mundschau G, Li Q, Fuchs E (2000). Conditional ablation of beta1 integrin in skin. Severe defects in epidermal proliferation, basement membrane formation, and hair follicle invagination. J Cell Biol 150, 1149–1160.
Rignol G, Garcia S, Authier F, Smith K, Tosello L, Marsault R, Dellugat P, Goncalves D, Brouillard M, Stavenhagen J, *et al.* (2022). Longitudinal Imaging of the Skull Base Synchondroses Demonstrate Prevention of a Premature Ossification After Recifercept Treatment in Mouse Model of Achondroplasia. JBMR Plus 6, e10568.
Romereim SM, Conoan NH, Chen B, Dudley AT (2014). A dynamic cell adhesion surface regulates tissue architecture in growth plate cartilage. Development 141, 2085–2095.
Rosello-Diez A, Joyner AL (2015). Regulation of long bone growth in vertebrates; it is time to catch up. Endocr Rev 36, 646–680.
Shum L, Wang X, Kane AA, Nuckolls GH (2003). BMP4 promotes chondrocyte proliferation and hypertrophy in the endochondral cranial base. Int J Dev Biol 47, 423–431.
Sissons H (1955). Experimental study on the effect of local irration on bone growth. Edinburgh, Scotland: Oliver & Boyd.
Stevens DG, Boyer MI, Bowen CV (1999). Transplantation of epiphyseal plate allografts between animals of different ages. J Pediatr Orthop 19, 398–403.

Tsang KY, Chan D, Cheah KS (2015). Fate of growth plate hypertrophic chondrocytes: death or lineage extension? Dev Growth Differ 57, 179–192.
Twitty VC, Schwind JL (1931). The growth of eyes and limbs transplanted heteroplastically between two species of Amblystoma. J Exp Zool 59, 61–86.
Unger CM, Devine J, Hallgrimsson B, Rolian C (2021). Selection for increased tibia length in mice alters skull shape through parallel changes in developmental mechanisms. eLife 10, e67612.
Wei X, Hu M, Mishina Y, Liu F (2016). Developmental regulation of the growth plate and cranial synchondrosis. J Dent Res 95, 1221–1229.
Wilson EB (1900). The Cell in Development and Inheritance. London, UK: The Macmillan Company, Norwood Press.
Yang G, Zhu L, Hou N, Lan Y, Wu XM, Zhou B, Teng Y, Yang X (2014). Osteogenic fate of hypertrophic chondrocytes. Cell Res 24, 1266–1269.
Yang L, Tsang KY, Tang HC, Chan D, Cheah KS (2014). Hypertrophic chondrocytes can become osteoblasts and osteocytes in endochondral bone formation. Proc Natl Acad Sci USA 111, 12097–12102.
Yano H, Mazaki Y, Kurokawa K, Hanks SK, Matsuda M, Sabe H (2004). Roles played by a subset of integrin signaling molecules in cadherin-based cell-cell adhesion. J Cell Biol 166, 283–295.
Young B, Minugh-Purvis N, Shimo T, St-Jacques B, Iwamoto M, Enomoto-Iwamoto M, Koyama E, Pacifici M (2006). Indian and sonic hedgehogs regulate synchondrosis growth plate and cranial base development and function. Dev Biol 299, 272–282.
Yuan J, Guo L, Wang J, Zhou Z, Wu C (2023). alpha-parvin controls chondrocyte column formation and regulates long bone development. Bone Res 11, 46.
Zhang Z, Sha B, Zhao L, Zhang H, Feng J, Zhang C, Sun L, Luo M, Gao B, Guo H, *et al*. (2022). Programmable integrin and N-cadherin adhesive interactions modulate mechanosensing of mesenchymal stem cells by cofilin phosphorylation. Nat Commun 13, 6854.
Zhou X, von der Mark K, Henry S, Norton W, Adams H, de Crombrugghe B (2014). Chondrocytes transdifferentiate into osteoblasts in endochondral bone during development, postnatal growth and fracture healing in mice. PLoS Genet 10, e1004820.